PAPER

# Design of Small CRPA Arrays for Dual-Band GPS Applications

Gangil BYUN[†], Seung Mo SEO[††], Ikmo PARK[†††], *Nonmembers*, *and* Hosung CHOO[††††a)], *Member*

**SUMMARY** This paper proposes the design of small CRPA arrays for dual-band Global Positioning System (GPS) applications. The array consists of five elements and is mounted on a circular ground platform with a diameter of 15-cm. Each antenna element has a coupled feed structure and consists of a feed patch and two radiating patches for dual-band operation. An external chip coupler is utilized for a broad circular polarization (CP) bandwidth, and its measured characteristics are taken into account in our simulation for more accurate performance estimation. Detailed parameters are optimized by using a genetic algorithm (GA) in conjunction with the FEKO EM simulator. The optimized antenna is fabricated on a ceramic substrate, and its performance is measured in a full anechoic chamber. Furthermore, a field test is also conducted to verify the signal-to-noise ratio (SNR) for real GPS satellite signals. The results prove that the proposed array is suitable for use in GPS CRPA applications.

***key words:*** *GPS antenna, CRPA array, coupled feed structure*

## 1. Introduction

The Global positioning system (GPS) has become essential in various applications that provide both the location and time information of moving objects, e.g., mobile devices, cars, ships, and aircraft. This system, however, fails to accurately track positions when the power of unwanted interference, such as multi-path signals, is stronger than that of the GPS satellite signals. To prevent this failure, controlled reception pattern antenna (CRPA) arrays have been investigated to increase the signal-to-noise ratio (SNR) of the system by placing adaptive pattern nulls in the directions of the sources of interference [1]–[4]. For CRPA operation, individual GPS antennas are often required to have multi-frequency operation, circular polarization (CP) properties, and wide-beam elevation coverage to receive satellite signals from low-elevation angles [5]. To satisfy these requirements, various types of antenna radiators, such as helical, conical, and spiral structures [6]–[9], have been investigated, but their physical characteristics may be an obstruction in an extremely small CRPA array; antennas are only permitted to be in a few centimeters in diameter and a few millimeters in height [10]. In searching for a more suitable candidate, microstrip patch antennas have been considered for a CRPA array because of their low profile characteristics [11]–[14]. The size of the antenna can be further improved by using a high-dielectric material as presented in [15], however, previous studies are limited to the design of a single antenna element without serious consideration of the mutual coupling effects among array elements, which often results in gain degradation, pattern distortions, or poor CP properties in such extremely small arrays [16]–[18]. In addition, previously reported dual-band antennas have difficulty in tuning their resonant frequencies separately, which is practically required in small CRPA arrays to realize good antenna performances.

In this paper, we propose the design of dual-band GPS antennas with a novel feeding mechanism for small CRPA arrays. The array consists of five antennas and is mounted on a circular ground platform with an inter-element spacing of about 52.9 mm ($< \lambda/4$, 1.2276 GHz). An individual array element has two radiating patches that are electromagnetically linked with the feed patch located between them. The feed patch is connected to an external chip coupler that is mounted on an FR4 substrate ($\varepsilon_r = 4.5$, $\tan\delta = 0.02$) using via-holes. By applying this feeding structure, the antenna achieves separate frequency tuning capability and high isolation between array elements, because it confines near electromagnetic fields to close proximity of the antenna. To estimate an accurate mismatch loss from the chip coupler and to improve the CP radiation gain, we apply a full scattering matrix measurement in the design process. A high-permittivity ceramic material is used for the antenna substrate, and its dielectric constant is determined by considering the antenna gain, aperture size, and mutual coupling between array elements. To improve the antenna's radiation gain even more, detailed parameters are optimized by using a genetic algorithm (GA) in conjunction with the FEKO EM simulator developed by EM Software and Systems [19], [20]. To verify the suitability of the proposed CRPA array, five optimized antennas are fabricated, and antenna characteristics, such as the reflection coefficient, radiation gains, and patterns, are measured in a full anechoic chamber. A field test is also conducted to measure the received SNR values for real GPS satellite signals. The results prove that the proposed array is suitable for use in GPS CRPA applications without causing any significant pattern distortions or gain degradations.

Manuscript received October 4, 2013.
Manuscript revised January 17, 2014.
[†]The author is with the Department of Electronics and Computer Engineering, Hanyang University, Seoul, Korea.
[††]The author is with Agency for Defense Development, Daejeon, Korea.
[†††]The author is with the School of Electrical and Computer Engineering, Ajou University, Suwon, Korea.
[††††]The author is with the School of Electronic and Electrical Engineering, Hongik University, Seoul, Korea.
a) E-mail: hschoo@hongik.ac.kr
DOI: 10.1587/transcom.E97.B.1130

## 2. Antenna Structure and Optimization

### 2.1 Individual Antenna Structure

Figure 1(a) shows the proposed multi-layer antenna structure with a coupled feed network for dual-band operation. The antenna consists of a feed patch, an L1 patch, and an L2 patch, each of which is printed on a ceramic substrate ($\varepsilon_r$ = 15.6, $\tan\delta$ = 0.0035). A substrate with appropriate relative permittivity is chosen by considering both the antenna aperture size and the coupling among the array elements. The L1 patch is square-shaped with edge length $W_1$, which is designed to be approximately half the effective wavelength in the L1 band. The same design scheme is applied for the L2 patch length ($W_2$) to achieve the L2 band resonance. These two patches are stacked to be electromagnetically coupled with the feed patch located between them. The coupling strength is then controlled by the size of the feed patch ($W_3$) and the substrate heights ($H_1$, $H_2$, and $H_3$). To attain broad CP characteristics, a chip coupler from Anaren (XC1400P-03S) is employed at the bottom of the FR4 substrate ($\varepsilon_r$ = 4.5, $\tan\delta$ = 0.02, and $H_4$ = 0.8 mm), as presented in Fig. 1(b). Two feed pins are linked to the chip coupler by using a coplanar waveguide and are connected to the feed patch through via holes. The two feeding positions, expressed as $x$- and $y$-coordinates, are determined to form a 90° angular difference between their position vectors, which is a well-known CP technique for a two-port feed network. Figure 1(c) shows the five-element circular array mounted on the circular platform with a diameter of 150 mm. The antennas are arranged on the outer perimeter of the platform to maintain the maximum isolation characteristics in the given area: the average isolation value between neighboring elements is about 18.36 dB in the two bands.

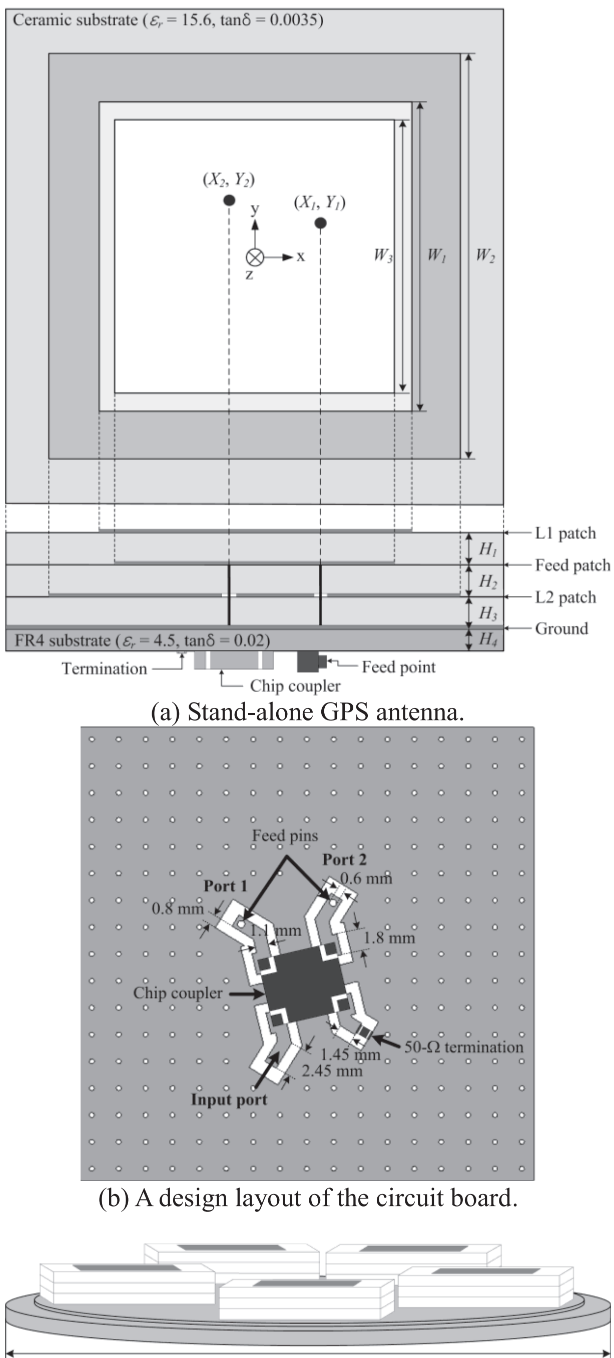

(a) Stand-alone GPS antenna.
(b) A design layout of the circuit board.
(c) CRPA array.

**Fig. 1** Proposed antenna structure.

Figure 2(a) shows triangular meshes of the CRPA array applied in the FEKO EM simulator, and Fig. 2(b) shows a picture of the fabricated CRPA array. To estimate accurate antenna performance within a short simulation time, the size of the mesh triangles is locally re-adjusted by considering the current distributions. For example, denser mesh triangles are utilized for the geometry near the feed ports, while coarse mesh triangles are employed for the array platform because of the low current distributions. As a result, the geometry of the entire antenna array is remodeled as approximately 5,500 piecewise mesh triangles, and a simulation time of approximately 10 minutes is achieved for each frequency point on a computer with an Intel Core i7-3820 quad-core processor and 64 GB of RAM. In our EM simulation, the antenna is excited by using two wire ports representing two feed pins from the coupler. It is assumed that the input powers of all ports are equal, and the phase difference between the ports is set to 90°, which is the ideal operation of the coupler. Array characteristics, such as pattern distortions, gain degradations, and isolation, are then observed by terminating four other array elements with 50-Ω loads.

### 2.2 Coupler Analysis

The chip coupler used in our design consists of four ports; the input, termination, and two output ports. The input port is the observation point of the total reflection coefficient of the antenna, and the termination port should be connected to a 50-Ω load. Ideally, the chip delivers half of its power to each output port with a phase difference of 90°. Equation (1) represents the ideal scattering matrix for this cou-

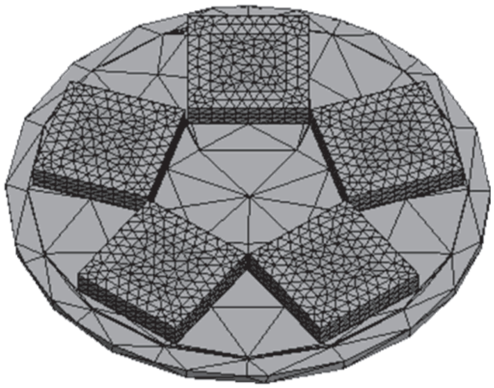

(a) Mesh triangles.

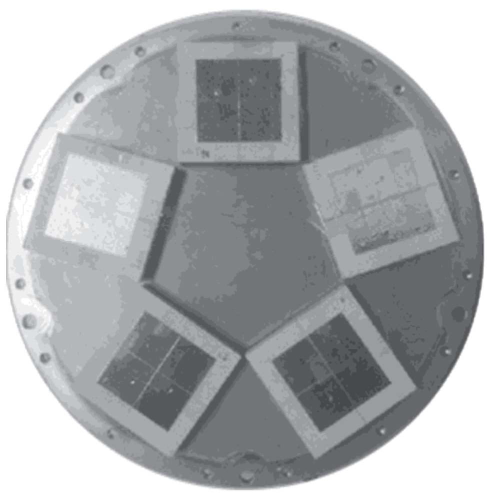

(b) Fabricated antennas.

**Fig. 2** Geometry of CRPA array.

pler operation, and Eq. (2) is the simulated scattering matrix for the antenna with a two-port feed network. Given these equations, the reflection coefficient of the input port can be calculated by Eq. (3).

$$\overline{S_{c,ideal}} = \frac{1}{\sqrt{2}} \begin{bmatrix} 0 & j & 1 & 0 \\ j & 0 & 0 & 1 \\ 1 & 0 & 0 & j \\ 0 & 1 & j & 0 \end{bmatrix} \quad (1)$$

$$\overline{S_{a,sim}} = \begin{bmatrix} S_{11} & S_{12} \\ S_{21} & S_{22} \end{bmatrix} \quad (2)$$

$$|\Gamma_{c,ideal}| = \frac{1}{2}\{(-S_{11} + S_{22}) + j(S_{12} + S_{21})\} \quad (3)$$

However, the real characteristics of the chip coupler, such as power reflection, division, and isolation, are a function of frequency, as shown in Fig. 3. Thus, we translate these measured data into a set of new scattering matrices for our design. Equation (4) shows an example at 1.5754 GHz. The matrices are then adapted by the Ansys Designer as a four-port network to revise the input reflection coefficient [21].

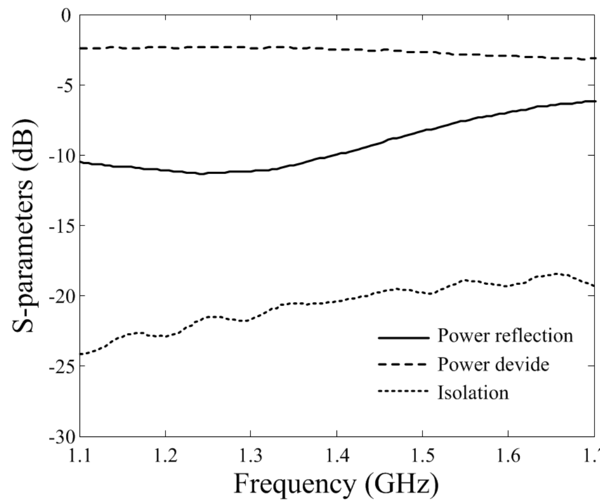


**Fig. 3** Measured characteristics of a chip coupler.

$$\overline{S_{c,meas}} = \begin{bmatrix} 0.29 & j0.51 & 0.20 & 0.07 \\ j0.51 & 0.29 & 0.07 & 0.20 \\ 0.20 & 0.07 & 0.29 & -0.23 + j0.46 \\ 0.07 & 0.20 & j0.51 & 0.29 \end{bmatrix} \quad (4)$$

### 2.3 GA Optimization

To further improve the radiation gain as well as the impedance matching characteristics, the proposed individual antenna structure is optimized by the GA in conjunction with the FEKO EM simulator. The cost function used in our optimization is shown in Eq. (5), and it is defined to raise the average CP gain of the antenna. In the equation, $G_{L1}$ and $G_{L2}$ are the CP gains of the upper hemisphere ($0° < \theta < 90°$) in the GPS L1 and GPS L2 bands, respectively, and $N_\varphi$ and $N_\theta$ represent the number of evaluated values of $\varphi$ and $\theta$, respectively. Some designs are excluded in our optimization when the mutual coupling between the array elements is greater than 12 dB, or the half power beamwidth (HPBW) is smaller than 90°.

$$\text{Cost } 1 = \frac{1}{\frac{1}{2}\left(\frac{1}{N_\varphi N_\theta \sum_{\theta=1}^{N_\theta}\sum_{\varphi=1}^{N_\varphi}} G_{L1}(\varphi,\theta) + \frac{1}{N_\varphi N_\theta}\sum_{\theta=1}^{N_\theta}\sum_{\varphi=1}^{N_\varphi} G_{L2}(\varphi,\theta)\right)} \quad (5)$$

Table 1 lists the optimized antenna parameters. The edge lengths of the L1 and the L2 patches, denoted by $W_1$ and $W_2$, are optimized to be slightly smaller than half of the effective wavelength in the each frequency band, because the radiating patches become more inductive due to the coupling in the proposed feeding mechanism. The two feeding positions are optimized to have an angle difference of 92.7° between their position vectors, enabling the antenna to be well phase-matched to the chip coupler with a 90° phase difference at its output ports.

**Table 1** Parameters of the optimized antenna.

| Parameter | Length |
|---|---|
| $W_1$ | 23.7 mm |
| $W_2$ | 31.2 mm |
| $W_3$ | 21.0 mm |
| $X_1$ | 5.5 mm |
| $X_2$ | −2.2 mm |
| $Y_1$ | 2.5 mm |
| $Y_2$ | 4.3 mm |
| $H_1$ | 2.5 mm |
| $H_2$ | 2.5 mm |
| $H_3$ | 2.5 mm |
| $H_4$ | 0.8 mm |

## 3. Measurement and Analysis

### 3.1 Antenna Performance

To verify the antenna performance, the optimized antenna is fabricated on the ceramic substrate (SMW-14, $\varepsilon_r = 15.6$, $\tan\delta = 0.0035$) obtained from Samboo Ceramics. The antenna is then mounted on a circular platform made of brass using a metal carving machine, and measurements are conducted in a full anechoic chamber (15.2 m (W) × 7.9 m (L) × 7.9 m (H)). Figure 4 shows the measured and simulated reflection coefficients of the antenna. The dashed line shows the estimated reflection coefficients with $S_{c,ideal}$, and the dotted line represents those with $S_{c,meas}$ shown in (4). As can be seen, the similarity between the measured and simulated coefficients, represented by a solid line, can be further improved by using the revised scattering matrix $S_{c,meas}$. Figure 5 shows the measured bore-sight gain of the antenna as a function of frequency. The figure shows that the antenna has a gain of approximately 0 dBic in the L1 band and −1.8 dBic in the L2 band.

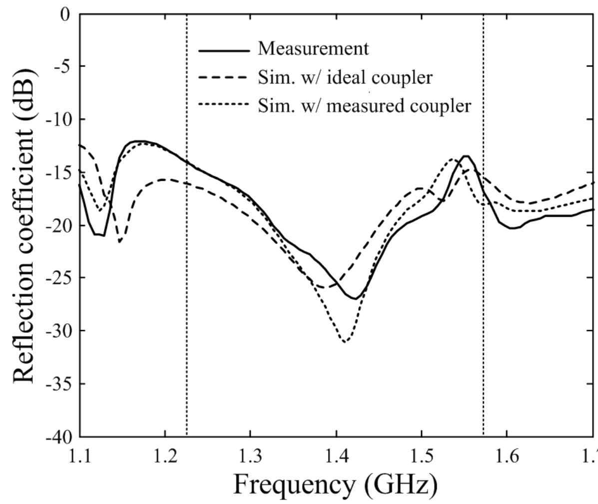


**Fig. 4** Reflection coefficient.

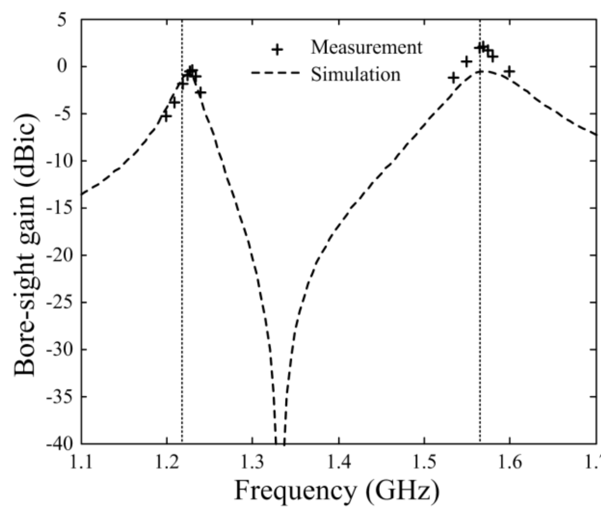


**Fig. 5** Bore-sight gain.

Figure 6 shows the measured radiation patterns in comparison with the simulation. Figures 6(a) and (b) show patterns in the *zx*- and *zy*-planes, respectively, at 1.5754 GHz, and their HPBWs are 117° and 138°, respectively. Figures 6(c) and (d) show the same planes at 1.2276 GHz with HPBWs of 96° and 112°, respectively. As can be observed, the antenna satisfies the HPBWs of greater than 90° without any serious gain degradation or pattern distortions in both frequency bands, which is suitable for use in a CRPA array application.

### 3.2 Interpretation

To analyze the operating principles of the antenna and to demonstrate its coupled feed structure from the circuit point of view, an equivalent circuit model is developed by a data fitting method to achieve the same impedance response that is obtained from $S_{11}$ presented in Eq. (3). The circuit and its detailed parameters are shown in Fig. 7(a). Although the three circuits, representing the feed patch, the L1 patch, and the L2 patch, are physically separated, they are inductively linked with each other by coupling coefficients $K_1$ and $K_2$. Figure 7(b) shows the input impedance of the circuit model in comparison with that of the EM simulation, and they agree well with each other. Figure 7(c) shows the coupling coefficients that are computed by solving the mesh equations of Kirchhoff's voltage law (KVL) in the frequency domain [22], [23]. As expected, the L1 patch is strongly linked with the feed patch at 1.575 GHz with the $K_1$ value of 0.6, and the L2 patch is coupled with the feed patch at 1.2276 GHz with the $K_2$ value of 0.35.

Figure 8 shows the H-field distributions in each band at the cross section ($y = 0$) to analyze the antenna in the field point of view. Figure 8(a) shows that there is a strong H-field distribution among the L1, feed, and L2 patches at 1.575 GHz, as observed in the circuit analysis. Figure 8(b) shows a strong H-field distribution between the L2 patch and the ground, which demonstrates that most of currents are induced on the L2 patch by the proposed feeding mechanism.

Figures 9(a) and (b) show variations of $S_{11}$ depending

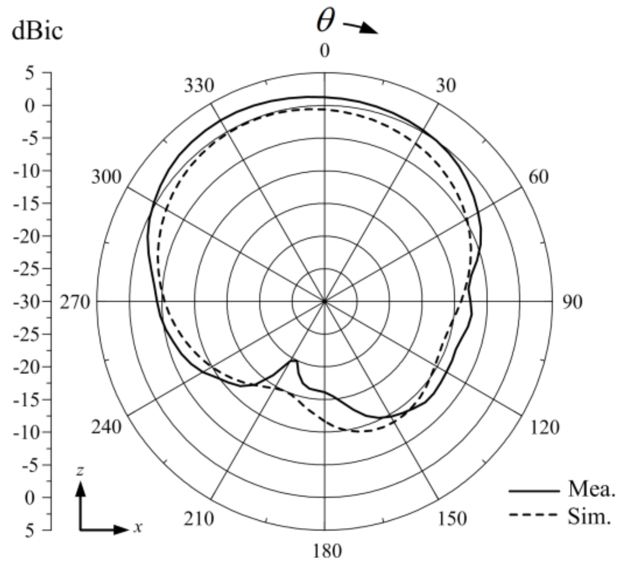

(a) *zx*-plane in L1 band.

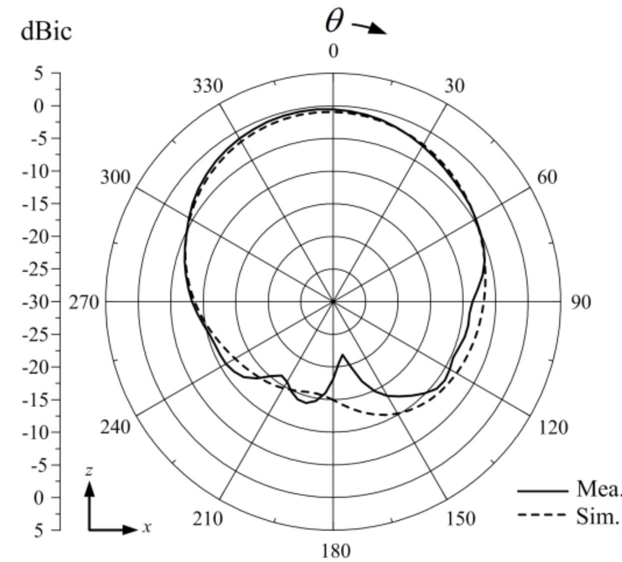

(c) *zx*-plane in L2 band.

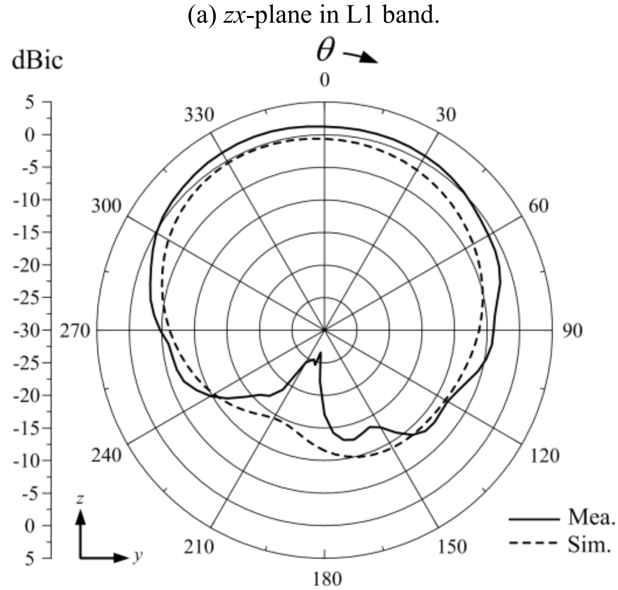

(b) *zy*-plane in L1 band.

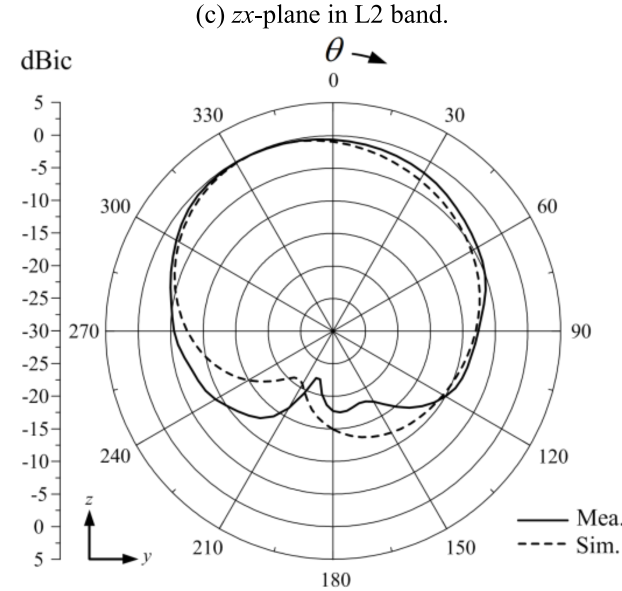

(d) *zy*-plane in L2 band.

**Fig. 6** Radiation patterns.

on the sizes of $W_1$ and $W_2$, respectively. As can be seen, the resonant frequency of the L2 patch does not vary due to the edge length of the L1 patch. The same phenomenon can be found in case of the L2 patch. Because of these phenomena, the frequency response of the bore-sight gains can also be adjusted by $W_1$ and $W_2$, as presented in Figs. 10(a) and (b).

### 3.3 Field Test

To demonstrate how the antenna operates functionally with a GPS receiver, we conducted a field test to measure the SNR values of the L-band GPS signals transmitted from real GPS satellites. Field measurements were conducted on a rooftop of a building (height = 13 m, Pangyo, Korea) in clear weather (temperature: 27.5°C, humidity: 62.6%). Figure 11(a) shows the GPS satellite positions recognized by the antenna. The antenna receives signals from 10 satellites that are located from $\theta = 25°$ to $\theta = 78°$. Figure 11(b) shows the measured SNR values for the satellites, each of which is specified with a space vehicle number. The measurements show an average SNR value of 12.7 dB with a maximum value of 18.5 dB. We can verify that the antenna is capable of receiving satellite signals at angles as high as $\theta = 78°$ with an SNR of 12.5 dB.

## 4. Conclusion

We have investigated the design of small CRPA arrays for dual-band GPS applications. The proposed individual antenna is composed of a feed patch, an L1 patch, and an L2 patch. The L1 and L2 patches were designed to resonate in the GPS L1 and GPS L2 bands, respectively, and are

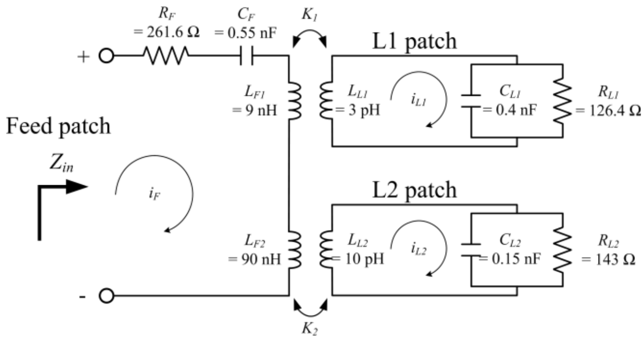

(a) Equivalent circuit model.

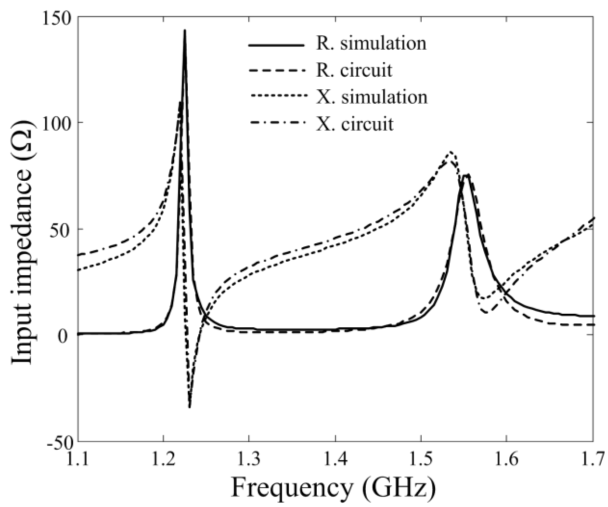

(b) Input impedance.

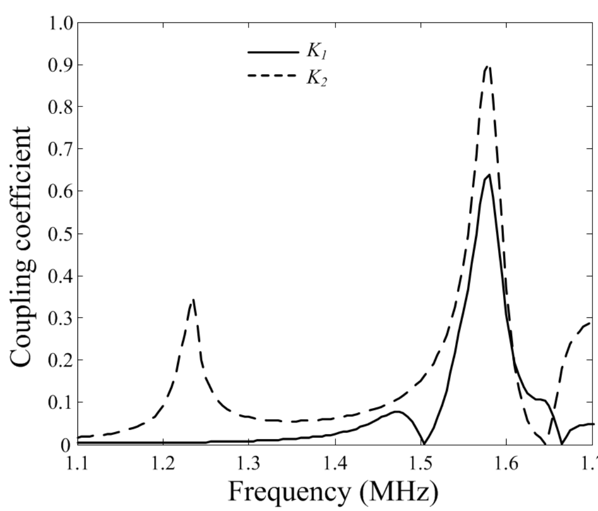

(c) Coupling coefficient.

**Fig. 7** Interpretation of the optimized antenna.

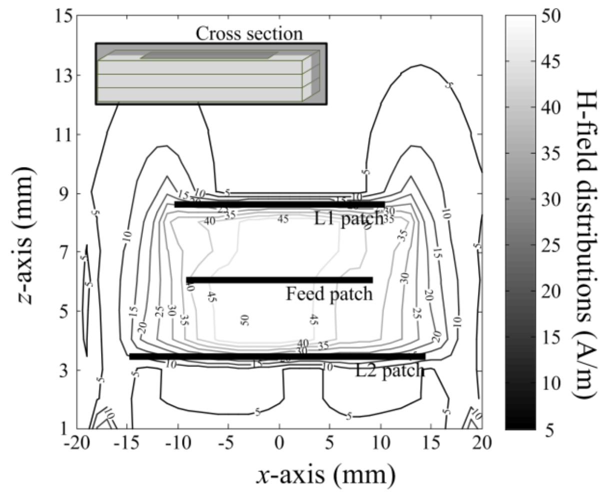

(a) L1 band.

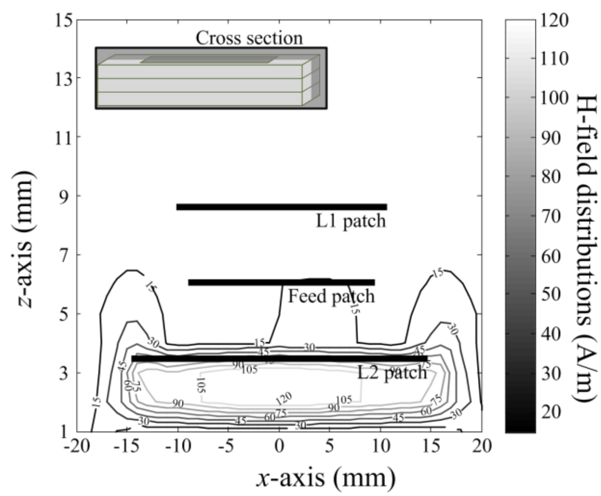

(b) L2 band.

**Fig. 8** H-field distrubution.

electromagnetically coupled to the feed patch located between them. The coupling strength was controlled by varying the substrate thickness to adjust the distance between the patches. The external chip coupler was used at the bottom of the antenna to achieve broad CP bandwidth, and its output ports were connected to the feed patch through via holes. In our simulation, the scattering matrix of the coupler was measured for more accurate performance estimation. The detailed parameters were optimized by using a GA in conjunction with the FEKO EM simulator. To verify the suitability of the proposed CRPA array, five optimized antennas were fabricated on the ceramic substrate and were installed on the outer perimeter of the 15-cm diameter circular platform. The antenna's characteristics were measured in a full anechoic chamber, and a field test was conducted at an open site to further verify the SNR values for real GPS satellite signals. The results proved that the proposed array is suitable for use in GPS CRPA applications with no significant pattern distortions or gain degradation.

**Acknowledgments**

This research was supported by the MSIP (Ministry of Science, ICT&Future Planning), Korea, under the ITRC (Information Technology Research Center) support program (NIPA-2013-H0301-13-2007) supervised by the NIPA (Na-

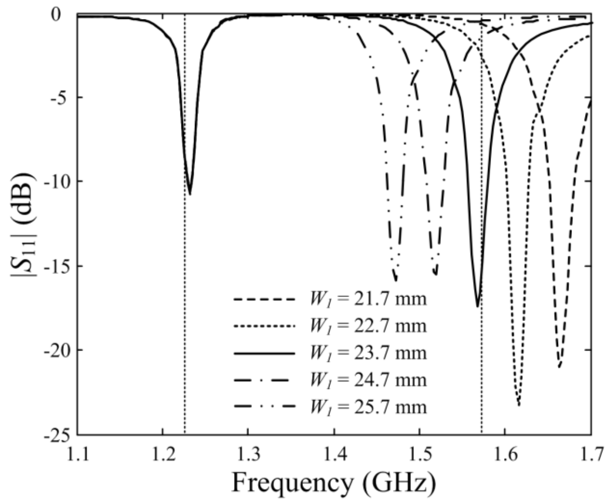


(a) $S_{11}$ according to $W_1$.

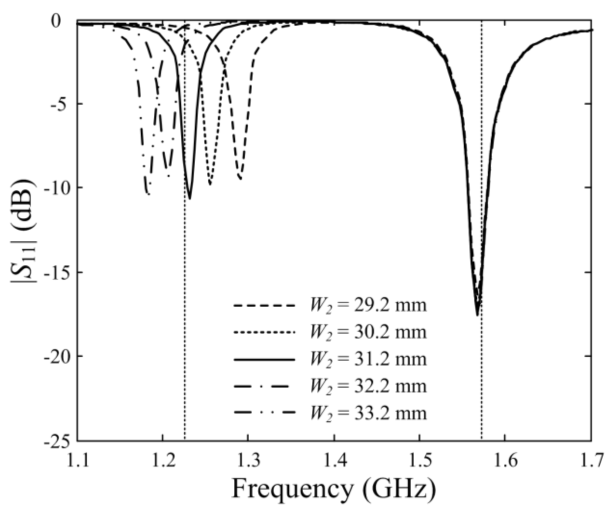


(b) $S_{11}$ according to $W_2$.

**Fig. 9** Variations of $S_{11}$.

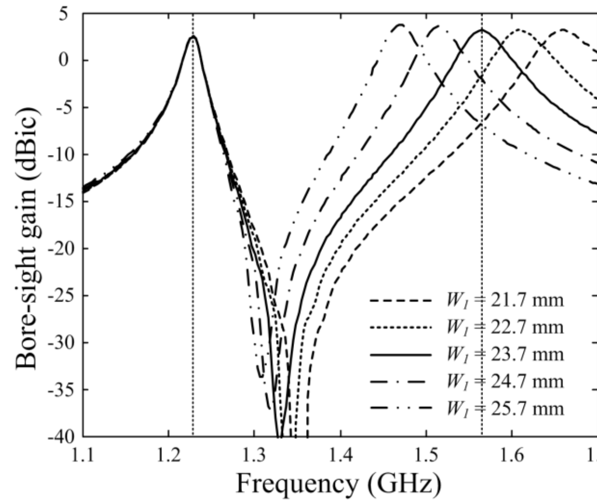


(a) Bore-sight gains according to $W_1$.

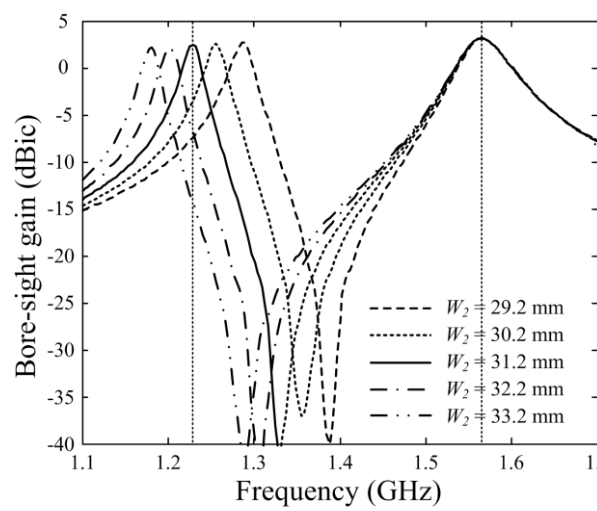


(b) Bore-sight gains according to $W_2$.

**Fig. 10** Variations of bore-sigh gains.

tional IT Industry Promotion Agency).

## References

[1] R. Fante and J.J. Vaccaro, "Wideband cancellation of interference in a GPS receive array," IEEE Trans. Aerosp. Electron. Syst., vol.36, no.2, pp.549–564, April 2000.

[2] Y. Zhang and M.G. Amin, "Array processing for nonstationary interference suppression in DS/SS communications using subspace projection techniques," IEEE Trans. Signal Process., vol.49, no.12, pp.3005–3014, Dec. 2001.

[3] M.G. Amin, L. Zhao, and A.R. Lindesy, "Subspace array processing for the suppression of FM jamming in GPS receivers," IEEE Trans. Aerosp. Electron. Syst., vol.40, no.1, pp.80–92, Jan. 2004.

[4] Y.D. Zhang and M.G. Amin, "Anti-jamming GPS receiver with reduced phase distortions," IEEE Process. Lett., vol.19, no.10, Oct. 2012.

[5] J.R. Lambert, C.A. Balanis, and D. DeCarlo, "Spherical cap adaptive antennas for GPS," IEEE Trans. Antennas Propag., vol.57, no.2, pp.406–413, Feb. 2009.

[6] J.M. Tranquilla and S.R. Best, "A study of the quadrifilar helix antenna for global positioning system (GPS) applications," IEEE Trans. Antennas Propag., vol.38, no.10, pp.1545–1550, Oct. 1990.

[7] P.K. Shumaker, C.H. Ho, and K.B. Smith, "Printed half wavelength quadrifilar helix antenna for GPS marine applications," Electron. Lett., vol.32, no.3, pp.153–154, Feb. 1996.

[8] N. Padros, J.I. Ortigosa, J. Baker, M.F. Iskander, and B. Thornberg, "Comparative study of high-performance GPS receiving antenna designs," IEEE Trans. Antennas Propag., vol.45, no.4, pp.698–706, April 1997.

[9] J. Rabemanantsoa and A. Sharaiha, "Size reduced multi-band printed quadrifilar helical antenna," IEEE Trans. Antennas Propag., vol.59, no.9, pp.3138–3143, Sept. 2011.

[10] J.G. Maloney, B.N. Baker, J.J. Acree, J.W. Schultz, J.A. Little, and D.D. Reuster, "Fragmented aperture antenna design of miniaturized GPS CRPA: Model and measurements," Proc. IEEE Antennas and Propagation Soc. Int. Symp., pp.3784–3787, Honolulu, USA, June 2007.

[11] L. Boccia, G. Amendola, and G.D. Massa, "A dual frequency microstrip patch antenna for high-precision GPS applications," IEEE Antennas Wireless Propag. Lett., vol.3, pp.157–160, 2004.

[12] J. Jan and K. Wong, "A dual band circularly polarized stacked elliptic microstrip antenna," Microwave Opt. Technol. Lett., vol.24, no.5, pp.354–357, March 2000.

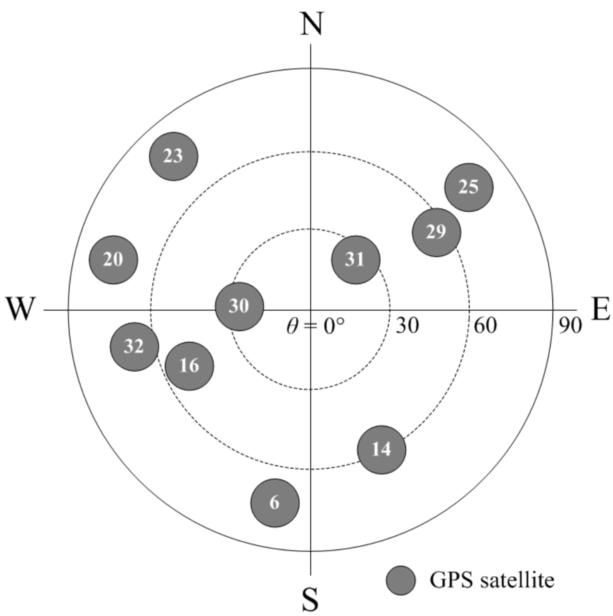

(a) GPS satellite positions.

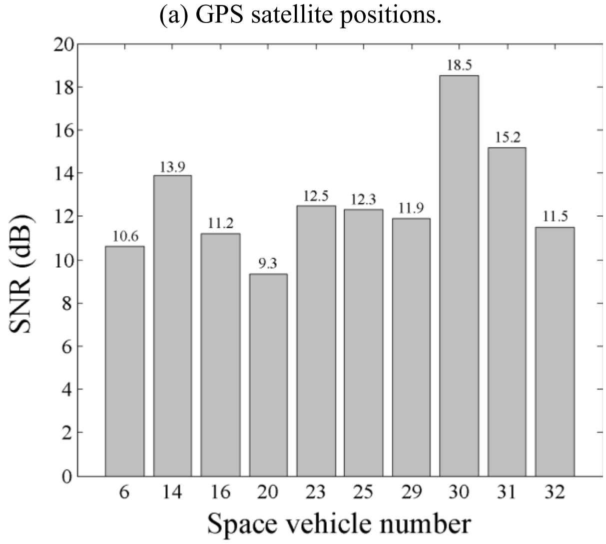

(b) Measured SNR values.

**Fig. 11** Field test results.

[13] S.Y. Lin and K.C. Huang, "A compact microstrip antenna for GPS and DCS application," IEEE Trans. Antennas Propag., vol.AP-53, pp.1227–1229, March 2005.

[14] K.P. Yang and K.L. Wong, "Dual-band circularly-polarized square microstrip antenna," IEEE Trans. Antennas Propag., vol.49, no.3, pp.377–382, March 2001.

[15] S.C. Chen, G.C. Liu, X.Y. Chen, T.F. Lin, X.G. Liu, and Z.Q. Duan, "Compact dual-band GPS microstrip antenna using multilayer LTCC substrate," IEEE Antennas Wireless Propag. Lett., vol.9, pp.421–423, May 2010.

[16] D.M. Pozar and S.M. Duffy, "A dual-band circularly polarized aperture-coupled stacked microstrip antenna for global positioning satellite," IEEE Trans. Antennas Propag., vol.45, no.11, pp.1618–1625, Nov. 1997.

[17] X. Sun, Z. Zhang, and Z. Feng, "Dual-band circularly polarized stacked annular-ring patch antenna for GPS application," IEEE Antennas Wireless Propag. Lett., vol.10, pp.49–52, 2011.

[18] C.A. Balanis, Theory: Analysis and Design, 3rd ed., Wiley, New York, 2005.

[19] FEKO Suite 6.1, EM Software and Systems, http://www.feko.info, accessed May 29. 2013.

[20] Y. Rahmat-Samii and E. Michielssen, Electromagnetic optimization by genetic algorithms, Wiley, New York, 1999.

[21] Ansys Designer v2.2, Ansys, Inc., http://www.ansys.com, accessed May 29. 2013.

[22] G. Byun, C. Seo, B.-J. Jang, and H. Choo, "Design of aircraft on-glass antennas using a coupled feed structure," IEEE Trans. Antennas Propag., vol.60, no.4, pp.2088–2093, April 2012.

[23] C.K. Alexander and M.N.O. Sadiku, Fundamentals of Electric Circuits, 2nd ed., McGraw-Hill, 2004.

**Gangil Byun** (S'12) was born in Seoul, Korea, in 1984. He received the B.S. and M.S. degrees in electronic and electrical engineering from Hongik University, Seoul, Korea, in 2010 and 2012, respectively. He is currently working toward the Ph.D. degree in electronics and computer engineering at Hanyang University, Seoul, Korea. His research interests include the design of aircraft antennas, global positioning system antennas, antenna arrays, and position optimization of array elements for adaptive beamforming applications.

**Seung Mo Seo** received the B.S. degree from Hong-Ik University, in 1998 and the M.S. and Ph.D. degree from The Ohio State University in 2001 and 2006, respectively, all in electrical engineering. From 1999 to 2006, he was Graduate Research Associate with the ElectroScience Laboratory (ESL), Department of Electrical and Computer Engineering, The Ohio State University, Columbus, where he focused on development of fast integral equation methods. From 2007 to 2010, he was Senior Engineer at DMC R&D Center, Samsung Electronics, where he developed RF circuit and antenna design and simulation. From 2011 to the present, he has been Senior Researcher at Agency for Defense Development. His current research interest is anti-jamming satellite navigation system.

**Ikmo Park** received the B.S. degree in Electrical Engineering from the State University of New York at Stony Brook, and M.S. and Ph.D. degrees in Electrical Engineering from the University of Illinois at Urbana-Champaign. He joined the Department of Electrical and Computer Engineering at Ajou University in March, 1996. Prior to joining Ajou University, he has been working with the Device & Materials Laboratory of LG Corporate Institute of Technology, Seoul, Korea, where he had been engaged in research and development of various antennas for personal communication systems, wireless local area networks, and direct broadcasting systems. He was a Visiting Professor with the Department of Electrical and Computer Engineering, POSTECH, Pohang, Korea, from March 2004 to February 2005, and the Department of Electrical and Computer Engineering, University of Arizona, Tucson, Arizona, USA, from July 2011 to June 2012. He has authored and co-authored over 200 technical journal and conference papers. He also holds over 30 patents. He served as a Chair of the Department of Electrical and Computer Engineering at Ajou University. He is a member of Board of Directors in the Korea Institute of Electromagnetic Engineering and Science. His current research interests include the design and analysis of microwave, millimeter-wave, terahertz wave, and nano-structured antennas. He is also a member of Eta Kappa Nu and Tau Betta Pi.

**Hosung Choo** (S'00, M'04, SM'11) was born in Seoul, Korea, in 1972. He received the B.S. degree in radio science and engineering from Hanyang University in Seoul in 1998, and the M.S. and Ph.D. degrees in electrical and computer engineering from the University of Texas at Austin, in 2000 and 2003, respectively. In September 2003, he joined the school of electronic and electrical engineering, Hongik University, Seoul, Korea, where he is currently an associate professor. His principal areas of research are the use of the optimization algorithm in developing antennas and microwave absorbers. His studies include the design of small antennas for wireless communications, reader and tag antennas for RFID, and on-glass and conformal antennas for vehicles and aircraft.